Advanced Quantum Technologies

ADVANCED QUANTUM TECHNOLOGIES
www.advquantumtech.com

RESEARCH ARTICLE OPEN ACCESS

Telecom C-Band Source of Triggered Polarization-Entangled Photon Pairs Combining High Coincidence Rates, Fidelities and Single-Photon Purity

Raphael Joos[1] | Mohamed Helal[2] | Michal Vyvlečka[1] | Lena Engel[1] | Aditi Javali[1] | Benjamin Breiholz[1] | Ponraj Vijayan[1] | Johannes Michl[2] | Michael Jetter[1] | Sven Höfling[2] | Tobias Huber-Loyola[2,3] | Giora Peniakov[2] | Simone L. Portalupi[1] | Peter Michler[1]

[1]Institut für Halbleiteroptik und Funktionelle Grenzflächen (IHFG), Center for Integrated Quantum Science and Technology (IQST) and SCoPE, University of Stuttgart, Stuttgart, Germany | [2]Physikalisches Institut, Lehrstuhl für Technische Physik, Julius-Maximilians-Universität Würzburg, Würzburg, Germany | [3]Institute of Photonics and Quantum Electronics (IPQ) and Center for Integrated Quantum Science and Technology (IQST), Karlsruhe Institute of Technology, Karlsruhe, Germany

Correspondence: Raphael Joos (r.joos@ihfg.uni-stuttgart.de) | Mohamed Helal (mohamed.helal@uni-wuerzburg.de)

Received: 9 January 2026 | **Revised:** 23 April 2026 | **Accepted:** 12 May 2026

Keywords: entanglement | quantum dots | telecom C-band

ABSTRACT

Many protocols of future quantum networks rely on the availability of entangled qubits which enable links among remote nodes due to their unique properties. Therefore, the efficient generation of entangled photons constitutes a key goal toward the implementation of such quantum networks. However, currently available sources are bound by intrinsic limitations, as for instance probabilistic nature of emission. Deterministic quantum emitters pose a potential solution for this issue, however, the maturity of their device platforms still needs to be improved for truly on-demand emission. While record efficiencies are currently found at near-infrared wavelengths, sources at telecommunication wavelengths will likely be the ideal choice for quantum networks. That motivates the development of efficient sources of entangled photons in the telecom regime. This work addresses that challenge presenting a telecom C-band source of polarization entangled photons based on semiconductor quantum dots incorporated in a planar cavity structure. In this way, triggered emission of entangled photon pairs with a coincidence rate of 201 ± 13 kcps (biexciton/exciton fiber-coupled single-photon count rates of 5.04 ± 0.16 Mcps/1.97 ± 0.06 Mcps) combined with $g^{(2)}(0)$ values of $0.009 \pm 0.001/0.015 \pm 0.001$ is achieved. Full quantum state tomography of the two-photon state demonstrates simultaneously entanglement fidelities of up to 0.964 ± 0.001 to the Φ^+ Bell state.

1 | Introduction

After decades of fundamental theoretical [1, 2] as well as experimental [3–7] research on quantum communication protocols, advances in technologies facilitate more and more real-world implementations of these well-understood applications [8–10]. The natural platform of qubits for these applications is given by photons due to their ability to bridge large distance at speed of light. Especially photonic quantum entanglement constitutes a key resource for many protocols, for instance BBM92 [11, 12]. For large scale quantum networks, however, the realization of quantum repeaters presents an important cornerstone to overcome inevitable transmission losses [13, 14]. For this, entangled photons constitute one of the most important resources for quantum repeaters [15], often in combination with atomic memories [16] allowing for synchronization of e.g. entanglement swapping

[Correction added on May 29, 2026, after first online publication: The copyright line was changed.]

processes [17, 18]. While experiments in a laboratory environment as well as out-of-the-lab demonstrations of entanglement-based implementations have been realized [19–21] the scalability of the quantum networks depends heavily on the availability of high-quality sources of entangled photons. For decades spontaneous parametric down-conversion (SPDC) sources have been the backbone of generation of entangled photon pairs [22, 23]. However, for SPDC sources the multiphoton-contribution and pair generation efficiency are fundamentally linked due to their probabilistic nature of light generation [24]. For this reason, potentially deterministic sources of entangled photon pair generation have attracted major research interest. For this purpose, semiconductor quantum dots (QDs) [25–27] constitute a promising candidate via their natural platform for entanglement generation, the biexciton–exciton cascade. These sources promise high achievable rates, high entanglement fidelities as well as mature fabrication technologies which allow for monolithic fabrication of microcavities. While QDs emitting at near-infrared wavelengths have shown remarkable performance as entangled photon pair sources [21, 28–31], QDs emitting at the telecom C-band, only allowing for long-distance fiber-based communication [32], have not yet been able to match these characteristics. So far entanglement generation from QDs at the telecom C-band has been shown on a fundamental research level [33, 34] enabling even first applications [35, 36], however the overall efficiency of the sources was still limited. The efficiency of QD sources can be strongly enhanced by cavity structures. For entanglement generation the cavity mode has to be, however, broad enough to accommodate the biexciton as well as exciton transition lines. For this reason, circular Bragg grating cavities (CBG) are considered as highly appealing structures since they allow for a high, broadband extraction efficiency with moderate Purcell enhancement. This enables coupling of both transition lines to the same cavity mode [30, 31]. Furthermore, telecom C-band CBGs have been demonstrated as efficient single-photon sources [37–39]. However, CBGs are prone to fabrication imperfections due to their very high demands on spatial positioning [40] and structural symmetry [41] which can affect the emitted polarization state ultimately limiting entanglement fidelities. Only recently, also limitations of the entangled state by the collection parameters have been reported for CBGs [42].

Here, we demonstrate the development of a high-brightness QD-source of entangled photon pairs emitting at the telecom C-band based on a planar cavity. Contrary to CBGs, in-plane symmetry is inherently guaranteed for planar cavities and the collection geometry does not affect the degree of entanglement [42] constituting a more robust sample design. The source is based on InAs QDs grown on a metamorphic buffer (MMB) layer and embedded in a planar λ-cavity structure consisting of semiconductor (top) as well as dielectric (bottom) distributed Bragg reflector (DBR) mirrors. The QDs are driven under resonant two-photon excitation (TPE) which enables accurate preparation of the biexciton state. In this way, high coincidence rates of 201 ± 13 kcps (biexciton/exciton fiber-coupled single-photon countrates of 5.04 ± 0.16 Mcps/1.97 ± 0.06 Mcps) are combined with with entanglement fidelities of up to 0.964 ± 0.001 and low biexciton (exciton) $g^{(2)}(0)$ values of 0.009 ± 0.001 and 0.015 ± 0.001, respectively. These results push forward the current state-of-the-art for QD-based sources of entangled photons in the telecom C-band.

2 | Methods and Device Characterization

Figure 1a shows a scanning electron microscopy (SEM) picture of the sample structure with a sketched QD layer. The sample fabrication starts with the deposition of alternating pairs of an AlAs/GaAs DBR mirror on a GaAs substrate and the subsequent growth of a thin-film MMB [43] layer which provides the necessary strain reduction for telecom C-band QD emission on a GaAs substrate. After the growth of the InAs QD layer the deposition of 10 pairs of dielectric SiO_2/TiO_2 DBR mirror completes the planar λ-cavity structure. All semiconductor growth steps are performed via metal-organic vapor phase epitaxy whereas the dielectric DBR is formed via ion-beam sputtering deposition. In a final step, the sample is transferred on a carrier chip via a flip-chip process and the substrate is removed via a physical polishing as well as wet-chemical etching leaving 11 pairs of AlAs/GaAs as upper DBR layer.

In order to investigate the influence of the top DBR deposition and the subsequent flip-chip process as well as the performance of the final sample, 18 (21) QDs on the final cavity sample (as-grown sample before top DBR deposition) are investigated regarding their spectral properties. All 18 QDs on the final cavity sample are found within a sample area of 460x460 μm. The samples are operated in a cryostat at about 4 K and addressed via confocal μ-photoluminescence spectroscopy. For each QD the biexciton state is excited via resonant TPE which enables straightforward suppression of the excitation laser via volume Bragg grating (VBG) notch filters. Figure 1b shows the emission spectrum of an exemplary QD, from here on referred to as QD1, at π-pulse (see Supporting Information for Rabi oscillations) as well as the cavity mode under strong, non-resonant pumping. Across the entire sample area of about 4×4 mm only a minor change of the cavity center wavelength below the width of the spectral cavity mode is observed. The QD spectrum shows a clear fingerprint of a biexciton–exciton cascade observing only the two desired transitions, which show a good overlap with the cavity mode, whereas any other emission as well as the excitation laser are well suppressed.

Any asymmetry in the QD confinement potential leads to a splitting of the originally degenerate exciton states, the so-called fine-structure splitting (FSS) [44]. This FSS leads to a time-dependent two-photon state of the biexciton–exciton cascade of

$$\Psi(\tau) = \frac{1}{\sqrt{2}}\left(|H_{XX}H_X\rangle + e^{-i\frac{FSS}{\hbar}\tau}|V_{XX}V_X\rangle\right), \quad (1)$$

with τ the time delay between biexciton and exciton photon. In case of time-averaging over the entire exciton wave package in a fixed measurement basis, this results in a reduction of the degree of entanglement. Therefore, for each QD the FSS is analyzed in a next step. For this, detection-polarization resolved spectroscopy is performed revealing the size of each QD's FSS. Additionally, the polarization angle for H-polarization is extracted and depicted together with the FSS in Figure 1c. Both samples show moderate QD FSS with mean values of 52 ± 27 μeV (61 ± 31 μeV). While these average values would strongly limit applications due to the wide spread of the distribution, there is also a reasonable chance to find QDs with FSS in the few μeV range. QDs with

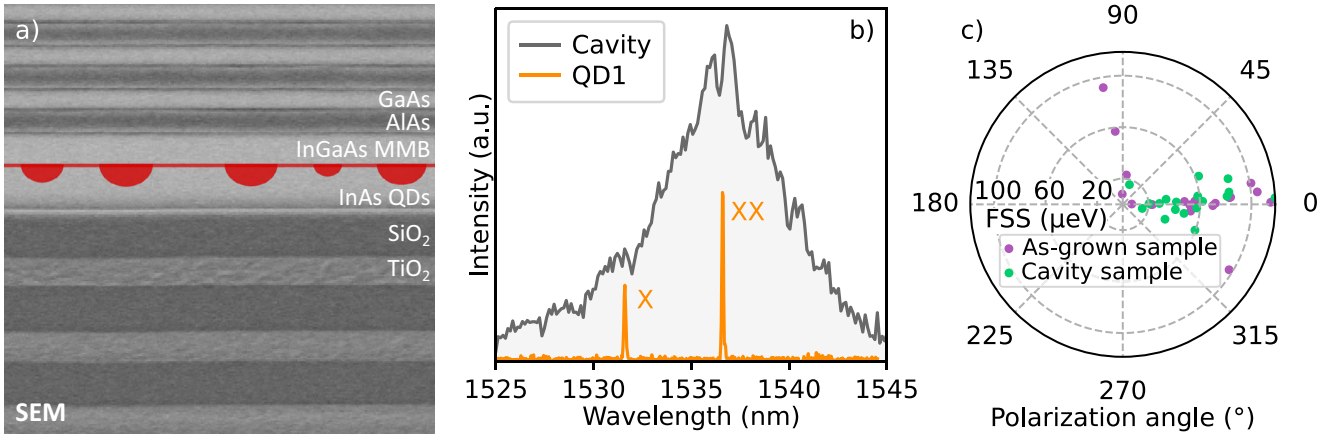

FIGURE 1 | (a) SEM picture and sketched QD layer of the sample structure. The final sample consists of InAs QDs in an MMB structure embedded in a planar cavity with 10 (11) pairs of TiO_2/SiO_2 (AlAs/GaAs) DBR mirrors. (b) Exemplary cavity spectrum under strong, non-resonant pumping and emission spectrum of QD1 under resonant two-photon excitation showing only biexciton (XX) and exciton (X) transition lines. (c) Fine-structure splitting and polarization angle of the H-component of the exciton emission for 18 QDs on the final cavity sample (green) and 21 QDs on the as-grown sample (violet).

such a FSS can be already interesting for certain applications [45]. Moreover, post-growth FSS tuning techniques as piezoelectric actuators [46, 47], electric [48] or magnetic fields [26] or even off-chip modulation [49] are easily compatible with this sample design potentially allowing for a full FSS erasure. Furthermore, from Figure 1c it is evident that the FSS of all QDs is aligned to mainly one axis (and a minor fraction to a second, 90∘-rotated axis). This indicates that the FSS is aligned with the crystal axes of the material, in turn suggesting that anisotropies in growth speed or strain relaxation along the different crystal axes are responsible for the FSS. The fabrication of the final cavity, however, does not seem to have any major influence on the strain acting on the QDs. Even though the FSS values found on these structures do not rule out real-world applications (especially together with potential post-growth FSS tuning techniques), growth optimizations toward higher QD symmetry [50, 51] are still appealing. This would increase the yield of low FSS QDs or decrease the technical complexity for said FSS tuning techniques.

3 | Quantum Optical Performance

After this description of the sample structure and statistics of the FSS metrics of the biexciton–exciton cascades for entanglement generation, in the following we will focus on the quantum optical properties of the emission. For this purpose, we discuss the performance of QD1, which shows a low FSS, with respect to the most relevant quantum optical properties for entangled photon pair sources, i.e. single-photon purity and entanglement fidelity of the emitted photons as well as the efficiency. QD1 is excited via resonant TPE whereas the excitation laser is suppressed with VBG notch filters and subsequently the exciton and biexciton are filtered individually with VBG bandpass filters as well as narrowband etalons (full-width at half maximum of 16 GHz). In order to unambiguously demonstrate the cascaded nature of the transition lines, a cross-correlation measurement is performed between the two lines. As shown in the inset of Figure 2a, cascaded emission between the two lines is clearly evidenced by the shape and the bunching behavior of the zero-delay peak.

Due to the FSS of QD1, the two-photon state of the biexciton–exciton cascade is time-dependent. This also allows to investigate the FSS of a QD in the temporal instead of spectral domain enabling a more precise determination of low FSS values due to fast single-photon detectors (Single Quantum Eos) and correlation electronics (Swabian Instruments TimeTagger Ultra). For this purpose, another cross-correlation measurement is carried out (see main frame of Figure 2a), where we project both, biexciton as well exciton, transitions onto D-polarization of the QD polarization eigenbasis. A fit to the data with the following Equation (2) (including a convolution which takes into account the full detection system's time jitter of 80 ps) yields an exciton decay time of 756 ± 2 ps as well as an oscillation period ($T_{\mathrm{FSS}} = \frac{h}{FSS}$) of 1287 ± 1 ps (FSS of about 3.21 μeV):

$$C(\tau) = A \cdot \Theta(\tau) \cdot \mathrm{e}^{-\frac{\tau}{T_{\mathrm{dec}}}} \cdot \left(1 + A_{\mathrm{osc}} \cdot \mathrm{e}^{-\frac{\tau}{T_{\mathrm{damp}}}} \cdot \cos\left(2\pi \frac{\tau}{T_{\mathrm{FSS}}}\right)\right) + B \tag{2}$$

A and B are the amplitude and background level of the signal while the heaviside function $\Theta(\tau)$ and the decay time T_{dec} describe the exponential decay of the exciton state. Please note that A_{osc} and T_{damp} are rather heuristic parameters motivated by the imperfection and damping of the oscillation rather than a precise theoretical model but still ensure a well-converging fit for precise determination of the decay time and the FSS.

Ideally, the cascaded emission process generates exactly one photon for the biexciton and one for the exciton. However, laser leakage, re-excitation of the system or spectral background might lead to multiphoton contributions for each detection channel. In order to investigate these influences, the single-photon purity of the individual transition lines is probed via photon autocorrelation measurements in a Hanbury–Brown and Twiss (HBT) interferometer setup, as depicted in Figure 2b. As anticipated from resonant TPE [52], for both transitions the zero-delay peak is strongly suppressed showing highly pure single-photon emission with $g^{(2)}(0)$ values of 0.009 ± 0.001 and 0.015 ± 0.001 for the biexciton and exciton, respectively.

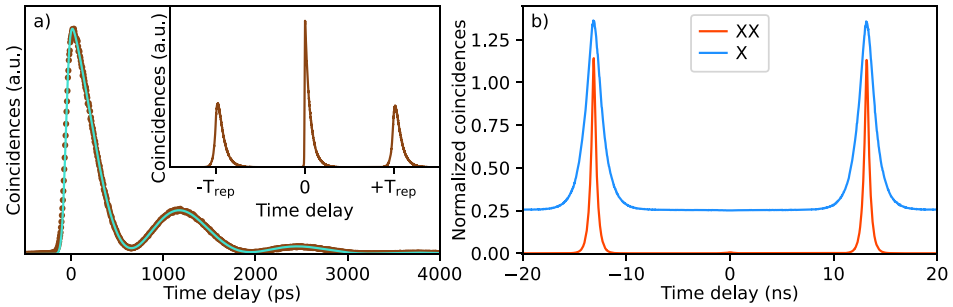

FIGURE 2 | (a) Biexciton–exciton cross-correlation measurements of QD1. The inset shows the full cross-correlation of both transitions while the main frame depicts cross-correlation only between D-polarized photons. A fit to the oscillations (turquoise line) yields an oscillation period of 1287 ± 1 ps (FSS of about 3.2 μeV). (b) Photon autocorrelation measurements of QD1 with an HBT setup of the biexciton transition (red) and the exciton transition (blue) yielding $g^{(2)}(0)$ values of 0.009 ± 0.001 and 0.015 ± 0.001, respectively. The exciton data are offset vertically by 0.25 for better visual clarity.

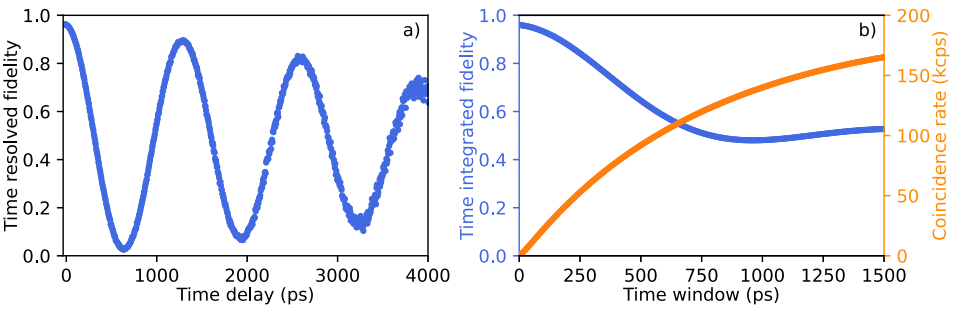

FIGURE 3 | (a) Time evolution of the fidelity toward the Bell state Φ^+ for a fixed window of 5 ps at different time delays for QD1. (b) Fidelity toward the Bell state Φ^+ for an increasing time window starting at zero time delay as well as coincidence rate within that time window for QD1.

Finally, the degree of entanglement of the emitted photon pairs is investigated. For this purpose, quantum state tomography [53] is employed where we measure the biexciton–exciton cross-correlation for all possible 36 combinations of polarization projections to {H, V, D, A, L, R} for both transitions. From the outcome of those measurements the two-photon density matrix is reconstructed by means of a maximum likelihood estimation [53, 54]. From this density matrix, the entanglement fidelity toward the Bell state Φ^+ is calculated and the time evolution the fidelity is depicted in Figure 3a for a fixed time window of 5 ps, however with increasing time delay between biexciton and exciton photon. As expected, the entanglement fidelity oscillates with the FSS oscillation period of 1287 ps due to the coherent phase evolution between the two exciton fine-structure states [55]. Furthermore, an overall damping of the fidelity over time is observed in Figure 3a. This can be mainly ascribed to decoherence mechanisms as spin-scattering as well as cross-dephasing between the two exciton states which reduces the overall degree of entanglement [55, 56]. This instantaneous evolution of the entanglement fidelity demonstrates how the two-photon state changes over time. For applications in quantum communication, though, often the state fidelity for an increasing integration time window of time delays between biexciton and exciton is interesting. Therefore, we discuss in the following this very merit as well as the coincidence rate (see Figure 3b). Due to the time-averaging, the fidelity does not drop as fast in this scenario showing that moderately high fidelities can be obtained even when considering a substantial fraction of the emission of QD1, for instance 25 % of the coincidences with a fidelity of 0.842 ± 0.001 (250 ps time window) or 50 % of the coincidences with a fidelity of 0.594 ± 0.001 (570 ps time window). However, more sophisticated quantum communication protocols could involve several coincidence windows around the maxima of the fidelity curves in Figure 3a (in case of adaptations of the bases even the minima can be used since they typically coincide with high fidelity toward the Φ^--state). This can increase the coincidence rate significantly without any technical overload. And even further, if it is possible to fully resolve the phase evolution (for instance with a rotating measurement basis), all coincidences can be used [45] with limitations on the fidelity arising only from the minor decoherence of the quantum state which is, however, beyond the decay time of the exciton state.

As mentioned above, the employed resonant TPE allows for efficient spectral filtering of the emission. Combined with the planar cavity arrangement this enables high efficiency operation of the entangled photon pair source. After all filtering elements (detailed discussion of the setup efficiency can be found in the Supporting Information) as well as incoupling into a single-mode optical fiber, a coincidence rate of 201 ± 13 kcps (corrected for the detection efficiency) (pair efficiency of 0.27 ± 0.02 %) is observed at a repetition rate of 76 MHz for QD1. At the same time, the fiber-coupled single-photon countrate of biexciton and exciton are determined as 5.04 ± 0.16 Mcps (efficiency of 6.64 ± 0.21 %) and 1.97 ± 0.06 Mcps (efficiency of 2.60 ± 0.08 %), respectively. This constitutes the highest efficiency and rates for telecom C-band

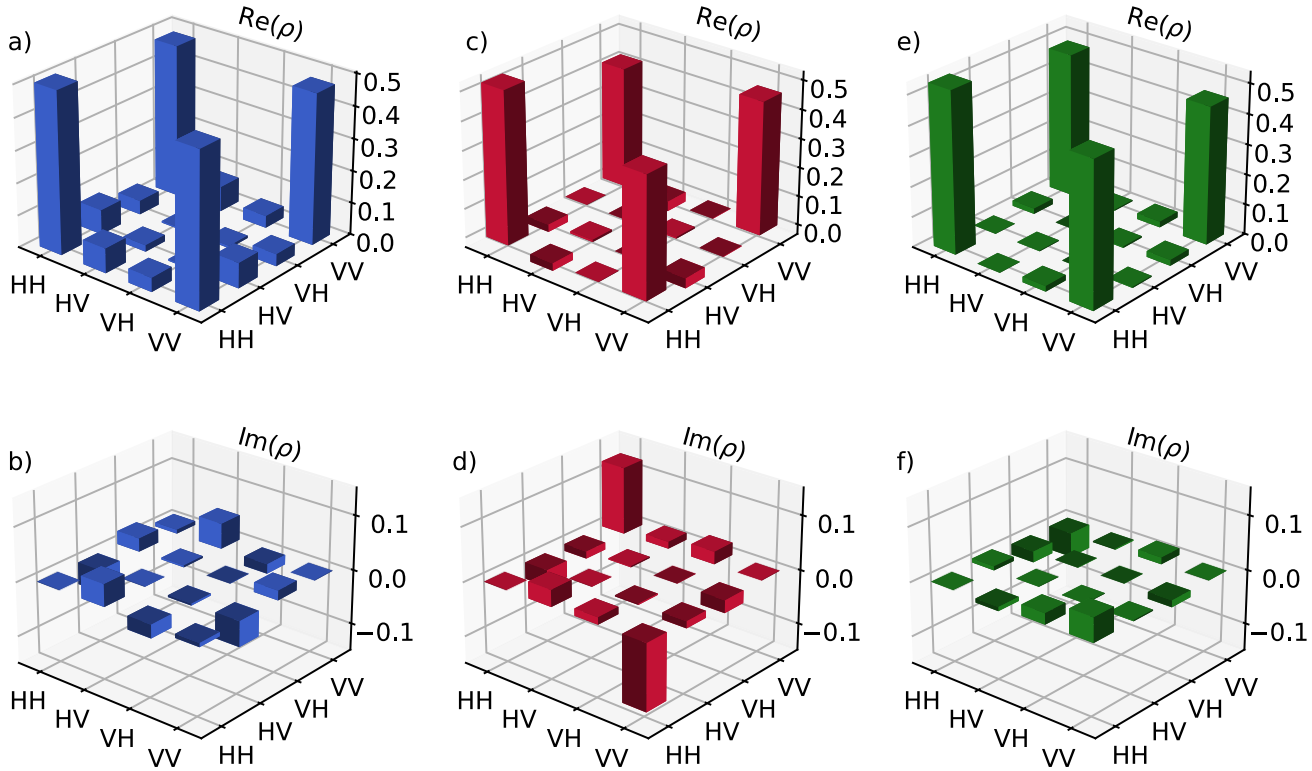

FIGURE 4 | Two-photon density matrices for QD1 (a/b), QD2 (c/d), QD3 (e/f) for a 5 ps (20 ps for QD3) time window. The top row shows the real and the bottom row the imaginary components.

QD entangled photon pair sources reported so far, estimating more than a ten-fold increase compared to the previous state-of-the-art [35, 36]. For QDs, only the best-performing sources based on CBG cavities at near-infrared wavelength achieve higher coincidence rates in a single-mode fiber of about 1 Mcps [31]. However, owing to post-growth FSS tuning techniques (in reference [31] via piezo electric actuators), these sources achieve high entanglement fidelities for the entire exciton wave packet. Implementation of piezo tuning of the FSS, which is already compatible with the sample design, could therefore be a next step toward telecom C-band sources of entangled photons with higher maturity. Nevertheless, this work denotes an important step toward closing the gap between the telecom sources and the more established near-infrared platform.

After the discussion of the time dependence and efficiency of the entangled photon pair generation, we conclude this study with a look at the two-photon state without consideration of the FSS oscillation, that means the density matrix at the maximum of the fidelity at zero phase (see Equation (1)). This is performed for QD1 as well as for two other QDs (QD2 and QD3) whereas QD3 is from a separate epitaxial growth and embedded in a structure with reversed DBR geometry (no-flip chip process and adjusted DBR reflectivities). Figure 4 shows the real (upper row) as well as imaginary parts (bottom row) of the obtained density matrices for a 5 ps (20 ps for QD3) time window. As anticipated from the theoretical form of the time-dependent two-photon state in Equation (1), the density matrices strongly resemble the Bell state Φ^+ with entanglement fidelities/concurrences [53] of $0.964 \pm 0.001/0.946 \pm 0.001$, $0.912 \pm 0.001/0.865 \pm 0.001$ and $0.975 \pm 0.002/0.956 \pm 0.005$ for QD1, QD2 and QD3, respectively. For QD2, the FSS induced oscillation of the state is explicitly fast with a period of 241 ± 1 ps. Due to the limited detection time resolution of 80 ps, this leads to a partial time-averaging of the state which we assume to be the main origin for the reduced fidelity of QD2 compared to the other QDs (see Supporting Information for time resolved fidelity and concurrence for QD1, QD2 and QD3). Beyond that, a high degree of entanglement is observed for multiple QDs on this structure constituting state-of-the-art performance for telecom C-band entangled photon pair sources based on QDs [34–36, 47].

4 | Conclusion

In this work, we present a telecom C-band source of entangled photon pairs based on semiconductor QDs in a planar cavity arrangement. SiO_2/TiO_2 and AlAs/GaAs DBR mirrors serve as bottom and top reflectors for the λ-cavity. Statistical investigations on 18 (21) QDs on the final cavity sample (as-grown sample before top DBR deposition and flip-chip process) show that there is no significant influence of the post-growth fabrication steps on the optical properties relevant for entanglement generation. We show detailed investigations of the quantum optical properties of one exemplary QD with an FSS of 3.2 μeV operated under resonant TPE. Full quantum state tomography of the two-photon polarization state is performed in all 36 basis combinations. This enables the time-resolved reconstruction of the photon pair's state demonstrating a maximum entanglement fidelity of 0.964 ± 0.001 toward the Bell state Φ^+. At the same time, the enhanced photon

extraction due to the planar cavity together with efficient spectral filtering of the emission enables a high entanglement rates with of 201 ± 13 kcps (biexciton/exciton fiber-coupled single-photon countrates of 5.04 ± 0.16 Mcps/1.97 ± 0.06 Mcps) combined with $g^{(2)}(0)$ values of $0.009 \pm 0.001/0.015 \pm 0.001$. These results constitute an important step forward toward the implementation of QD-based entangled photon sources in realistic quantum communication scenarios.

Acknowledgements

R. J. and M. H. contributed equally to this work. R. J., M. V., L. E., A. J., P. V., M. J., S. L. P. and P. M. acknowledge funding by the German Federal Ministry of Research, Technology and Space (BMFTR) via project QR.X (16KISQ013) and QR.N (16KIS2207). Additional funding was also provided via the project EQSOTIC. This project was funded within the QuantERA II Programme that has received funding from the EU's H2020 research and innovation programme under the GA No 101017733, and with funding organization BMFTR (with project number 16KIS2060K). M. H., J. M., S. H. and G. P. acknowledge funding by the BMFTR via the projects QR.N (16KIS2209) and PhotonQ (13N15759). T. H.-L. acknowledges funding by the BMFTR via the project QECS (13N16272).

Open access funding enabled and organized by Projekt DEAL.

Conflicts of Interest

The authors declare no conflicts of interest.

Data Availability Statement

The data that support the findings of this study are available from the corresponding author upon reasonable request.

References

1. C. H. Bennett and G. Brassard, "Quantum Cryptography: Public Key Distribution and Coin Tossing," *Theoretical Computer Science* 560, no. P1 (2014): 7–11.

2. H.-K. Lo, X. Ma, and K. Chen, "Decoy State Quantum Key Distribution," *Physical Review Letters* 94, no. 23 (2005): 230504.

3. J.-Y. Guan, J. M. Arrazola, R. Amiri, et al., "Experimental Preparation and Verification of Quantum Money," *Physical Review A* 97, no. 3 (2018): 032338.

4. Y. Liu, Y. Cao, M. Curty, et al., "Experimental Unconditionally Secure Bit Commitment," *Physical Review Letters* 112, no. 1 (2014): 010504.

5. N. H. Y. Ng, S. K. Joshi, C. Chen Ming, C. Kurtsiefer, and S. Wehner, "Experimental Implementation of Bit Commitment in the Noisy-Storage Model," *Nature Communications* 3, no. 1 (2012): 1326.

6. Y. Liu, Z.-W. Yu, W. Zhang, et al., "Experimental Twin-Field Quantum Key Distribution Through Sending or Not Sending," *Physical Review Letters* 123, no. 10 (2019): 100505.

7. A. Pappa, P. Jouguet, T. Lawson, et al., "Experimental Plug and Play Quantum Coin Flipping," *Nature Communications* 5, no. 1 (2014): 3717.

8. Y.-A. Chen, Q. Zhang, T.-Y. Chen, et al., "An Integrated Space-to-Ground Quantum Communication Network Over 4,600 Kilometres," *Nature* 589, no. 7841 (2021): 214–219.

9. M. Peev, C. Pacher, R. Alléaume, et al., "The SECOQC Quantum Key Distribution Network in Vienna," *New Journal of Physics* 11, no. 7 (2009): 075001.

10. T.-Y. Chen, X. Jiang, S.-B. Tang, et al., "Implementation of a 46-Node Quantum Metropolitan Area Network," *npj Quantum Information* 7, no. 1 (2021): 134.

11. C. H. Bennett, G. Brassard, and N. D. Mermin, "Quantum Cryptography Without Bell's Theorem," *Physical Review Letters* 68, no. 5 (1992): 557–559.

12. F. Xu, X. Ma, Q. Zhang, H.-K. Lo, and J.-W. Pan, "Secure Quantum Key Distribution with Realistic Devices," *Reviews of Modern Physics* 92, no. 2 (2020): 025002.

13. H.-J. Briegel, W. Dür, J. I. Cirac, and P. Zoller, "Quantum Repeaters: The Role of Imperfect Local Operations in Quantum Communication," *Physical Review Letters* 81, no. 26 (1998): 5932–5935.

14. L.-M. Duan, M. D. Lukin, J. I. Cirac, and P. Zoller, "Long-Distance Quantum Communication with Atomic Ensembles and Linear Optics," *Nature* 414, no. 6862 (2001): 413–418.

15. K. Azuma, S. E. Economou, D. Elkouss, et al., "Quantum Repeaters: From Quantum Networks to the Quantum Internet," *Reviews of Modern Physics* 95, no. 4 (2023): 045006.

16. P. van Loock, W. Alt, C. Becher, et al., "Extending Quantum Links: Modules for Fiber and Memory–Based Quantum Repeaters," *Advanced Quantum Technologies* 3, no. 11 (2020): 1–15.

17. M. Żukowski, A. Zeilinger, M. A. Horne, and A. K. Ekert, ""Event-Ready Detectors" Bell Experiment via Entanglement Swapping," *Physical Review Letters* 71, no. 26 (1993): 4287–4290.

18. T. van Leent, M. Bock, F. Fertig, et al., "Entangling Single Atoms Over 33 km Telecom Fibre," *Nature* 607, no. 7917 (2022): 69–73.

19. T. Jennewein, C. Simon, G. Weihs, H. Weinfurter, and A. Zeilinger, "Quantum Cryptography with Entangled Photons," *Physical Review Letters* 84, no. 20 (2000): 4729–4732.

20. J. Yin, Y.-H. Li, S.-K. Liao, et al., "Entanglement-Based Secure Quantum Cryptography Over 1,120 Kilometres," *Nature* 582, no. 7813 (2020): 501–505.

21. C. Schimpf, M. Reindl, D. Huber, et al., "Quantum Cryptography with Highly Entangled Photons from Semiconductor Quantum Dots," *Science Advances* 7, no. 16 (2021): eabe8905.

22. C. Couteau, "Spontaneous Parametric Down-Conversion," *Contemporary Physics* 59, no. 3 (2018): 291–304.

23. C. Zhang, Y. Huang, B. Liu, C. Li, and G. Guo, "Spontaneous Parametric Down-Conversion Sources for Multiphoton Experiments," *Advanced Quantum Technologies* 4, no. 5 (2021): 2000132.

24. J. Schneeloch, S. H. Knarr, D. F. Bogorin, et al., "Introduction to the Absolute Brightness and Number Statistics in Spontaneous Parametric Down-Conversion," *Journal of Optics* 21, no. 4 (2019): 043501.

25. N. Akopian, N. H. Lindner, E. Poem, et al., "Entangled Photon Pairs from Semiconductor Quantum Dots," *Physical Review Letters* 96, no. 13 (2006): 130501.

26. R. M. Stevenson, R. J. Young, P. Atkinson, et al., "A Semiconductor Source of Triggered Entangled Photon Pairs," *Nature* 439, no. 7073 (2006): 179–182.

27. R. Hafenbrak, S. M. Ulrich, P. Michler, L. Wang, A. Rastelli, and O. G. Schmidt, "Triggered Polarization-Entangled Photon Pairs from a Single Quantum Dot up to 30 K," *New Journal of Physics* 9, no. 9 (2007): 315–315.

28. M. Müller, S. Bounouar, K. D. Jöns, M. Glässl, and P. Michler, "On-Demand Generation of Indistinguishable Polarization-Entangled Photon Pairs," *Nature Photonics* 8, no. 3 (2014): 224–228.

29. Y. Chen, M. Zopf, R. Keil, F. Ding, and O. G. Schmidt, "Highly-Efficient Extraction of Entangled Photons from Quantum Dots Using a Broadband Optical Antenna," *Nature Communications* 9, no. 1 (2018): 2994.

30. J. Liu, R. Su, Y. Wei, et al., "A Solid-State Source of Strongly Entangled Photon Pairs with High Brightness and Indistinguishability," *Nature Nanotechnology* 14, no. 6 (2019): 586–593.

31. M. B. Rota, T. M. Krieger, Q. Buchinger, et al., "A Source of Entangled Photons Based on a Cavity-Enhanced and Strain-Tuned GaAs Quantum Dot," *eLight* 4, no. 1 (2024): 13.

32. Y. Yu, S. Liu, C.-M. Lee, et al., "Telecom-Band Quantum Dot Technologies for Long-Distance Quantum Networks," *Nature Nanotechnology* 18, no. 12 (2023): 1389–1400.

33. F. Olbrich, J. Höschele, M. Müller, et al., "Polarization-Entangled Photons from an InGaAs-Based Quantum Dot Emitting in the Telecom C-Band," *Applied Physics Letters* 111, no. 13 (2017): 133106.

34. K. D. Zeuner, K. D. Jöns, L. Schweickert, et al., "On-Demand Generation of Entangled Photon Pairs in the Telecom C-Band with InAs Quantum Dots," *ACS Photonics* 8, no. 8 (2021): 2337–2344.

35. G. Shooter, Z.-H. Xiang, J. R. A. Müller, et al., "1 GHz Clocked Distribution of Electrically Generated Entangled Photon Pairs," *Optics Express* 28, no. 24 (2020): 36838.

36. M. Anderson, T. Müller, J. Huwer, et al., "Quantum Teleportation Using Highly Coherent Emission from Telecom C-Band Quantum Dots," *npj Quantum Information* 6, no. 1 (2020): 14.

37. C. Nawrath, R. Joos, S. Kolatschek, et al., "Bright Source of Purcell-Enhanced, Triggered, Single Photons in the Telecom C-Band," *Advanced Quantum Technologies* 2300111 (2023): 1–6.

38. P. Holewa, D. A. Vajner, E. Zięba-Ostój, et al., "High-Throughput Quantum Photonic Devices Emitting Indistinguishable Photons in the Telecom C-Band," *Nature Communications* 15, no. 1 (2024): 3358.

39. J. Kaupp, Y. Reum, F. Kohr, et al., "Purcell-Enhanced Single-Photon Emission in the Telecom C-Band," *Advanced Quantum Technologies* 6, no. 12 (2023): 1–8.

40. G. Peniakov, Q. Buchinger, M. Helal, et al., "Polarized and Unpolarized Emission from a Single Emitter in a Bullseye Resonator," *Laser & Photonics Reviews* 18, no. 4 (2024): 1–7.

41. H. Wang, Y.-M. He, T.-H. Chung, et al., "Towards Optimal Single-Photon Sources from Polarized Microcavities," *Nature Photonics* 13, no. 11 (2019): 770–775.

42. A. Laneve, M. B. Rota, F. Basso Basset, et al., "Wavevector-Resolved Polarization Entanglement from Radiative Cascades," *Nature Communications* 16, no. 1 (2025): 6209.

43. R. Sittig, C. Nawrath, S. Kolatschek, et al., "Thin-Film InGaAs Metamorphic Buffer for Telecom C-Band InAs Quantum Dots and Optical Resonators on GaAs Platform," *Nanophotonics* 11, no. 6 (2022): 1109–1116.

44. M. Bayer, A. Kuther, A. Forchel, et al., "Fine Structure of Neutral and Charged Excitons in Self-Assembled In(Ga)As/(Al)GaAs Quantum Dots," *Physical Review Letters* 82, no. 8 (1999): 1748–1751.

45. M. Pennacchietti, B. Cunard, S. Nahar, et al., "Oscillating Photonic Bell State from a Semiconductor Quantum Dot for Quantum Key Distribution," *Communications Physics* 7, no. 1 (2024): 62.

46. R. Trotta, J. Martín-Sánchez, J. S. Wildmann, et al., "Wavelength-Tunable Sources of Entangled Photons Interfaced with Atomic Vapours," *Nature Communications* 7, no. 1 (2016): 10375.

47. T. Lettner, S. Gyger, K. D. Zeuner, et al., "Strain-Controlled Quantum Dot Fine Structure for Entangled Photon Generation at 1550 nm," *Nano Letters* 21, no. 24 (2021): 10501–10506.

48. A. Muller, W. Fang, J. Lawall, and G. S. Solomon, "Creating Polarization-Entangled Photon Pairs from a Semiconductor Quantum Dot Using the Optical Stark Effect," *Physical Review Letters* 103, no. 21 (2009): 217402.

49. A. Fognini, A. Ahmadi, S. J. Daley, M. E. Reimer, and V. Zwiller, "Universal Fine-Structure Eraser for Quantum Dots," *Optics Express* 26, no. 19 (2018): 24487.

50. Y. H. Huo, A. Rastelli, and O. G. Schmidt, "Ultra-Small Excitonic Fine Structure Splitting in Highly Symmetric Quantum Dots on GaAs (001) Substrate," *Applied Physics Letters* 102, no. 15 (2013): 152105.

51. D. Deutsch, C. Buchholz, V. Zolatanosha, K. D. Jöns, and D. Reuter, "Telecom C-Band Photon Emission from (In,Ga)As Quantum Dots Generated by Filling Nanoholes in In0.52Al0.48As Layers," *AIP Advances* 13, no. 5 (2023): 055009.

52. L. Schweickert, K. D. Jöns, K. D. Zeuner, et al., "On-Demand Generation of Background-Free Single Photons from a Solid-State Source," *Applied Physics Letters* 112, no. 9 (2018): 093106.

53. D. F. V. James, P. G. Kwiat, W. J. Munro, and A. G. White, "Measurement of Qubits," *Physical Review A* 64, no. 5 (2001): 052312.

54. Kwiat Quantum Information Group, https://pypi.org/project/Quantum-Tomography, version 1.0.7.0.

55. A. J. Hudson, R. M. Stevenson, A. J. Bennett, et al., "Coherence of an Entangled Exciton-Photon State," *Physical Review Letters* 99, no. 26 (2007): 266802.

56. D. Huber, M. Reindl, J. Aberl, A. Rastelli, and R. Trotta, "Semiconductor Quantum Dots as an Ideal Source of Polarization-Entangled Photon Pairs On-Demand: A Review," *Journal of Optics* 20, no. 7 (2018): 073002.

Supporting Information

Additional supporting information can be found online in the Supporting Information section.

Supporting File: qute70317-sup-0001-SuppMat.pdf.